Expression of Interest in Construction of an Off-Axis Near Detector to Measure Neutrino Cross Sections on Nuclear Targets In the Few GeV Region with the NUMI Beam

Arie Bodek, Howard Budd, Pawel de Barbaro, George Ginther, Steven Manly, Kevin McFarland,* Willis Sakumoto, Paul Slattery, and Marek Zielinski

High Energy and Nuclear Physics Groups
Department of Physics and Astronomy
University of Rochester, Rochester, NY 14627

June 4, 2002

Abstract

We investigate the possibility of constructing a near-source detector for the Fermilab NUMI neutrino beam with the purpose of measuring neutrino interactions and NUMI beam fluxes in the few GeV energy range. Such an experiment would be an important supporting part of the program to probe neutrino mixing, masses and CP violation through the observation of $\overset{(-)}{\nu}_\mu \to \overset{(-)}{\nu}_e$ transitions in low energy conventional neutrino beams.

---

*Scientific contact

Contents

1   Summary and Motivation

We propose to form a collaboration to construct a fully active off-axis near detector to measure charged-current and neutral-current cross sections with the Fermilab NUMI beam. The main purpose of the experiment is to perform high statistics measurements of neutral-current and charge-current neutrino interaction cross-sections on nuclear targets in the few GeV energy region. These measurements are of interest, both as crucial input to planned low energy neutrino oscillation experiments, and in their own right as a probe of nuclear structure.

The proposed near detector would to be located in a new experimental area off the access tunnel to the present MINOS on-axis near detector, about 880 meters from the production target, shown in Figure 1, at an angle with respect to the neutrino beam of about 11 mrad similar to that of the proposed off-axis long-baseline far detector[1] in the NUMI beam. NUMI would provide a beam with a peak energy of 2 GeV to such a detector. Ideally, the near detector should be movable so the off-axis angle can be changed; for example, a 23 mrad angle gives a peak neutrino energy of 1 GeV.

At first, the off-axis near detector will run parasitically with the MINOS experiment using the Low Energy (LE) beam configuration. The near off-axis detector sees nearly the same spectrum for both the LE and Medium Energy (ME) configuration currently planned for a future off-axis NUMI experiment.

Charged-current and neutral-current neutrino cross sections in the few GeV region will be measured in a fully-active 2 ton (fiducial volume) neutrino target and tracking calorimeter constructed from scintillator strips/bars with wavelength shifting fiber readout. At 2 GeV, cross-sections for quasi-elastic scattering, and CC and NC charged and neutral pion inelastic production cross-sections are all significant and measurable in such an experiment. These cross-sections are currently poorly measured and are necessary inputs for understanding signals and backgrounds observed in a low-energy neutrino long-baseline oscillation experiments.

For the proposed NUMI off-axis long-baseline experiment, this detector also plays a valuable role in measuring directly the backgrounds, both due to high energy NC interactions and electron neutrinos from the beam. The addition of detector and target material similar to proposed long-baseline detectors can enhance this detector's ability to serve as the monitor and test-bench for a future far detector. The proposed integrated active target design is modular and flexible. Target planes can be modified to use other target materials, and sampling fractions of a long-baseline off-axis far detector. Addition of other target materials will allow comparison of electron-scattering data on different nuclei to neutrino data with the same targets (e.g. carbon, iron, water) at the same energies.

Measurement of these cross-sections is also part of a collaborative effort with scientists currently involved in low-energy experiments at Jefferson Lab to fully measure and model neutrino-nucleon, neutrino-carbon, neutrino-nucleus and electron-nucleon, electron-carbon, and electron-nucleus reactions in the few GeV region. These data will provide the foundation for current and future precision neutrino oscillation experiments in the US, Japan and Europe.
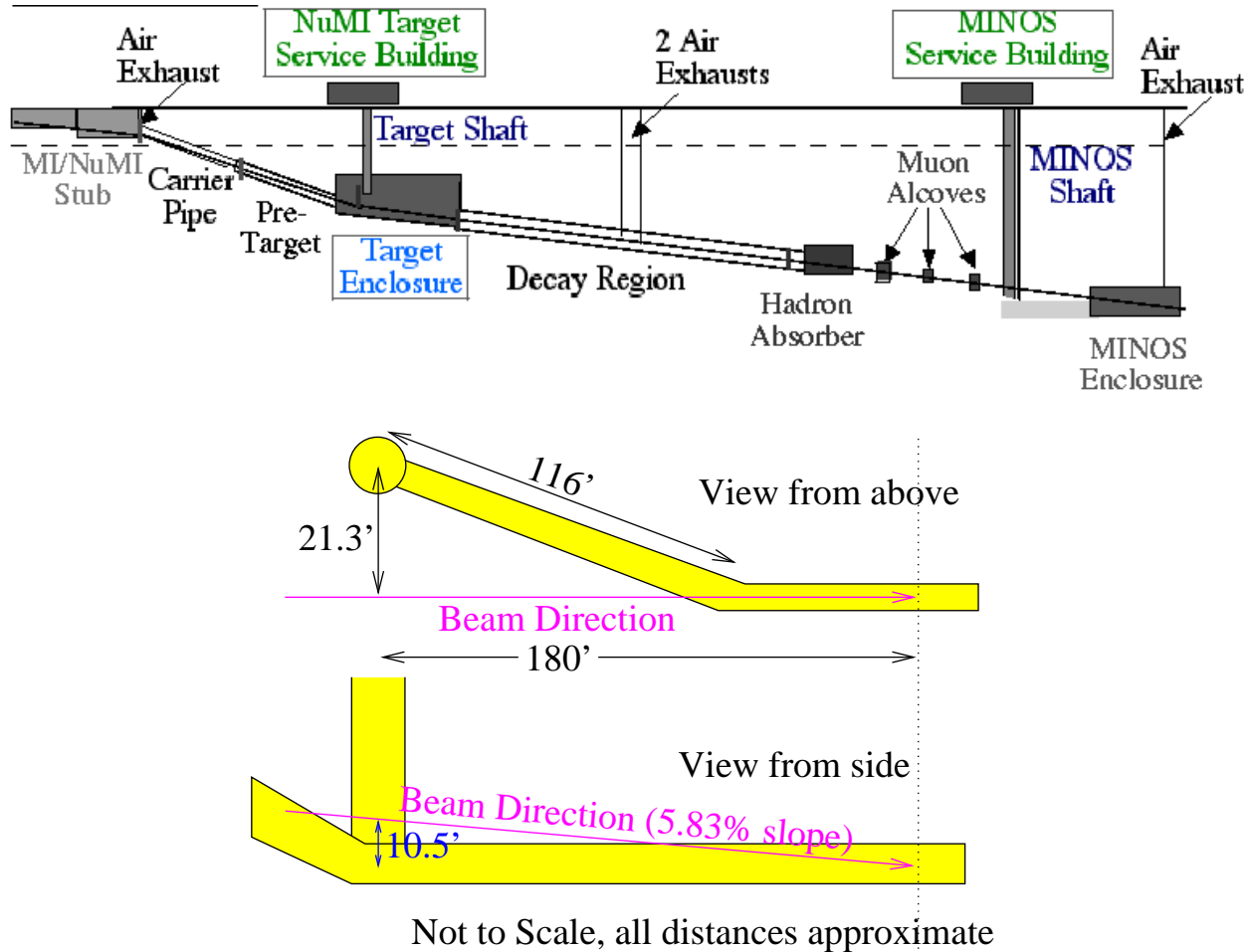
Figure 1: Access tunnel between the NUMI near detector hall and shaft. A new experimental hall located to the west of this tunnel would provide the correct location for the proposed new off-axis near detector.

1.1 Current status of neutrino oscillations

The roadmap for the neutrino physics program contains a number of branch points where new measurements will point the way to the long-term future goals[2]. The most convincing measurements of neutrino oscillation come from the up-down asymmetry of the atmospheric neutrino flux measured by the Super-Kamiokande experiment. The size of this asymmetry points to a nearly maximal neutrino mixing, and corroborating data indicates a mass splitting, $\delta m^2_{\text{atm}} \approx 3 \times 10^{-3}\text{eV}^2$, with most of the ν_μ disappearance into ν_τ[3]. Solar neutrinos provide a second measurement of neutrino oscillations, and recent evidence from the SNO experiment[4] suggests that the solar neutrino transition is primarily from ν_e into other active neutrinos. It also suggests that the solution to the solar neutrino deficit is a large mixing MSW solution with a $\delta m^2 \sim 5 \times 10^{-5}\text{eV}^2$. The very recent day/night asymmetry measurement from SNO offers direct evidence that this solution is correct, and these indications will be tested with high significance by the KAMLAND and Borexino experiments in the near future. The final and most controversial piece of evidence is the unconfirmed

signature of $\overline{\nu}_e$ appearance by the LSND experiment[5]. If LSND has also observed neutrino oscillations, then a fourth and therefore "sterile" neutrino must be involved, a possibility disfavored by the solar and atmospheric data.

Assuming above atmospheric and solar neutrino observations are correct and that the LSND signature is not confirmed by the upcoming BooNE experiment at Fermilab, then the MNS neutrino mixing matrix, parameterized as

$$U_{MNS} \approx \begin{pmatrix} C_{12}C_{13} & S_{12}C_{13} & S_{13}e^{-i\delta} \\ -S_{12}C_{23} - C_{12}S_{23}S_{13}e^{i\delta} & C_{12}C_{23} - S_{12}S_{23}S_{13}e^{i\delta} & S_{23}C_{13} \\ S_{12}S_{23} - C_{12}C_{23}S_{13}e^{i\delta} & -C_{12}S_{23} - S_{12}C_{23}S_{13}e^{i\delta} & C_{23}C_{13} \end{pmatrix}$$

has two large mixing angles, θ_{12} and θ_{23}, and one, θ_{13} that is small, to accommodate the absence of $\overline{\nu}_e$ disappearance in the CHOOZ and Palo Verde experiments[6, 7]. The mass splittings are also highly non-degenerate in this scenario, one with $\delta m^2 \sim 5 \times 10^{-5} \text{eV}^2$ and two with $\delta m^2 \approx 3 \times \sim 10^{-3} \text{eV}^2$. If $E_\nu/L \gg 10^{-4}$ eV^2, then the probability in vacuum for a flavor transitions suppressed by this small angle, e.g., $\nu_\mu \rightarrow \nu_e$, can be approximated as

$$P(\nu_\mu \rightarrow \nu_e) \approx \sin^2 2\theta_{13} \sin^2 \theta_{23} \sin^2 \left(\frac{\delta m^2_{\text{atm}} L}{4E} \right).$$

The effective two-generation mixing angle, $\theta_{\mu e}$ is defined so that

$$\sin^2 2\theta_{\mu e} \equiv \sin^2 2\theta_{13} \sin^2 \theta_{23}.$$

The atmospheric neutrino data favors a nearly maximal $\sin^2 2\theta_{23}$, so $\sin^2 \theta_{23} \approx 1/2$. A measurement of this transition probability therefore measures the small angle, $\sin \theta_{13} = |U_{e3}|$. The measurement of this sub-leading oscillation is analogous to searching for first and third generation mixing in the quark sector, which has led to a rich phenomenology of CP-violation, meson mixing and rare decays in the quark sector.

1.2   The Measurement of $\nu_\mu \rightarrow \nu_e$

If U_{e3} is in fact non-zero, then two important future measurements are possible. First, it is possible to determine directly the hierarchy of the neutrino masses by comparing $P(\nu_\mu \rightarrow \nu_e)$ to $P(\overline{\nu}_e \rightarrow \overline{\nu}_\mu)$ in matter[8]. This is not possible with vacuum oscillation measurements, because they probe only the magnitude of δm^2 and not the sign. However, the well-known matter enhancement of neutrino oscillations leads to a dependence in the transition probabilities on both the magnitude and sign of δm^2, thus allowing us to determine whether one small splitting implies two heavy and one light neutrinos or vice-versa.

The *pièce de resistance* of neutrino oscillation measurements is the search for CP violation in the MNS matrix. CP violation occurs when there are two amplitudes contributing to a given process with a relative phase, and therefore CP violation in neutrino oscillations requires that the θ_{13} and δ parameters in the MNS matrix are non-zero. Practically, observation at the L/E appropriate for δm^2_{atm} also requires a large $\delta m^2_{\text{solar}}$, such as in the large mixing-angle MSW solution so that the second contributing amplitude is not too small. This will be a challenging measurement and may
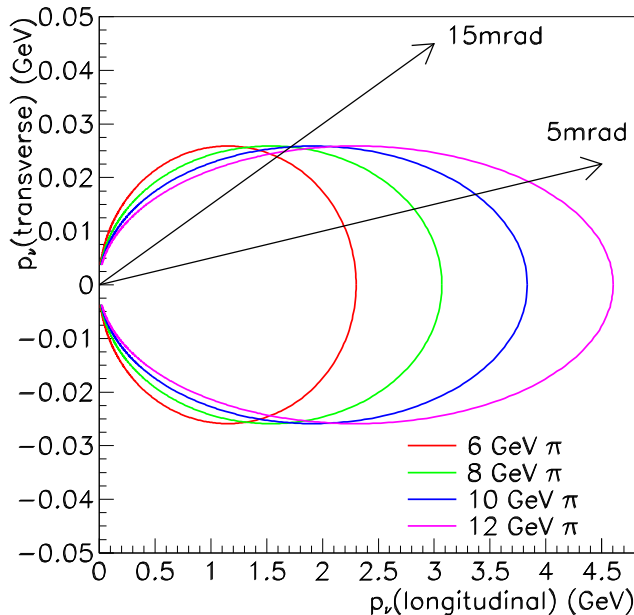
Figure 2: Schematic illustration of the off-axis beam technique. As can be seen, at a modest angle away from the focal axis of the pion beam (in this case, approximately 1° or 15 mr) pions of many different momenta all decay to neutrinos with approximately 1.5 GeV in an off-axis far detector.

ultimately require multi-megawatt beams and megaton size neutrino detectors, but the payoff in the end is potentially the observation of a profound connection between mixing in the quark and lepton sectors.

The first step on this roadmap is the observation of $U_{e3} \neq 0$ in the atmospheric δm^2 region. Conventional neutrino production, decay of mesons produced in proton fixed-target interactions, produces beams that are primarily muon neutrinos or anti-neutrinos. Therefore the discovery channel for U_{e3} is $\nu_\mu \to \nu_e$ and its charge conjugate. The desirable experimental characteristics in order to make a substantial improvement in U_{e3} past the CHOOZ bound are:

- $L/E \approx 4/\delta m^2_{\text{atm}} \sim 400$ km/GeV

- Low E_ν or highly active detector to reduce background from ν_μ neutral current interactions

- $> 10^3\ \nu_\mu$ charged current events in long-baseline detector (without oscillations)

The long-baseline experiments currently under construction, NUMI/MINOS and CNGS, can achieve the last of these criteria, but only at the cost of going to relatively high energy, which spoils the first two factors. Consequently, NUMI/MINOS and CNGS have very limited U_{e3} reach beyond the CHOOZ limit.

6

1.3 Off-axis Long Baseline Neutrino Experiments

Off-axis beams for neutrino oscillation experiments are highly desirable because they are nearly monochromatic. The reason for the narrow energy spectrum of such beams is illustrated schematically in Figure 2, which shows that charged pions of all energies decay to neutrinos of approximately equal energies at a fixed angle. This idea for beam construction is applicable and desirable for both long-baseline and short-baseline ("near") neutrino detectors.

Neutrino appearance and disappearance probabilities are functions of L/E only. Therefore, in long-baseline oscillation experiments, a narrow band beam of the correct energy results in maximal oscillation probabilities. Another important feature for massive detectors with difficulty in separating neutral-current (NC) interactions of muon neutrinos from charged-current (CC) reactions of other flavors of neutrinos is the ability to use visible energy as a discriminant. For CC events, the total neutrino energy is observed in the detector, but for NC events, the unobserved final state neutrino can carry off significant energy. Therefore, high energy NC events appear as oscillation candidates at lower energy. A monochromatic beam minimizes this "feed-down" background from NC interactions.

Currently, two $\nu_\mu \to \nu_e$ appearance experiments are being discussed using high-rate sources and off-axis neutrino beams. The first proposes to send an intense low energy neutrino beam from the 0.8 MWatt 50 GeV Proton Synchrotron (PS) currently being constructed at JAERI in Tokai, Japan to the existing Super-Kamiokande detector 295 km away[9], beginning as early as 2007. The beam for this experiment is a 2–3° off-axis beam with a peak energy of approximately 700 MeV. The second possible experiment, located at Fermilab, proposes to use the existing NUMI beam with a detector situated 0.6° off-axis at a distance of approximately 700 km[1]. This beam would have a peak energy of 2 GeV, thus making possible the observation of matter effects. However, another intriguing possibility for this proposal is to move further off-axis to a lower energy to run at the second maximum of the oscillation pattern where sensitivity to CP violating effects is enhanced.

Both experiments have potential upgrade paths to more intense proton sources and larger detectors should the initial running be successful in observing $|U_{e3}|$ and should other experiments make possible the future observation of leptonic CP violation.

2   Neutrino Fluxes in Off-Axis Detectors

For short-baseline experiments, a narrow band beam, particularly one that varies in a predictable way as a function of angle from the source, is valuable for measuring neutrino cross-sections, since incoming neutrino spectrum is well-known. This allows relative reaction rates to be measured as a function of energy in a straightforward manner.

The resulting off-axis neutrino beams are somewhat lower in rate and significantly lower in energy than conventional on-axis neutrino beams. Figure 3 shows the difference between the observed neutrino energy spectrum in the planned MINOS [10] near on-axis detector and an off-axis (0.6°) long-baseline NUMI detector. By contrast,
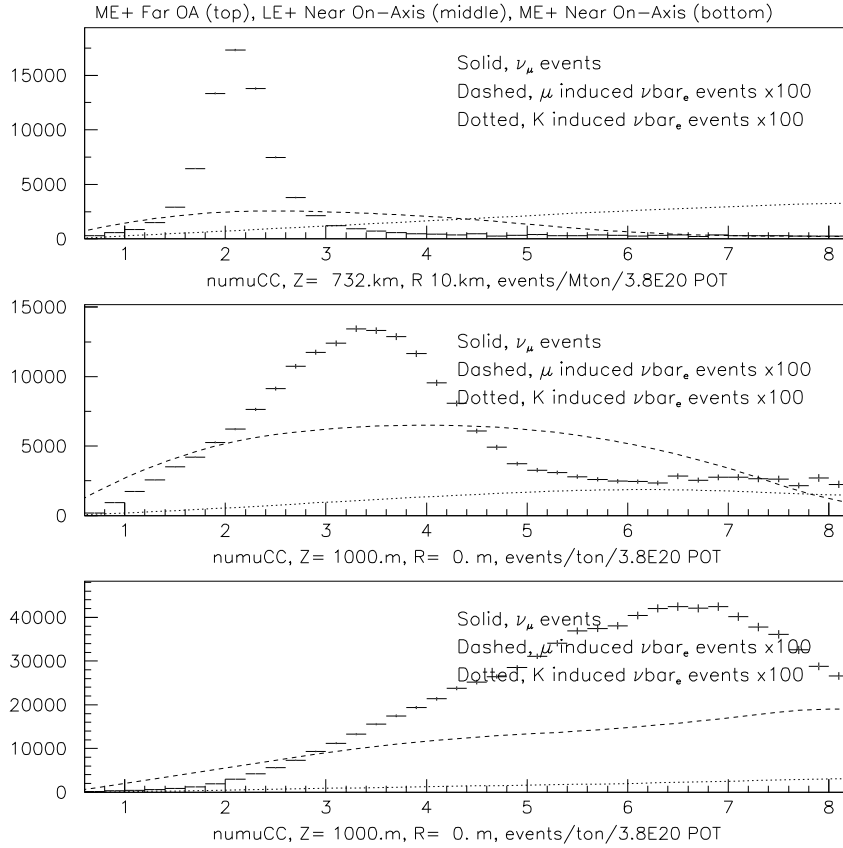
ME+ Far OA (top), LE+ Near On—Axis (middle), ME+ Near On—Axis (bottom)

Solid, ν_μ events
Dashed, μ induced $\overline{\nu} bar_e$ events x100
Dotted, K induced $\overline{\nu} bar_e$ events x100

numuCC, Z= 732.km, R 10.km, events/Mton/3.8E20 POT

Solid, ν_μ events
Dashed, μ induced $\overline{\nu} bar_e$ events x100
Dotted, K induced $\overline{\nu} bar_e$ events x100

numuCC, Z= 1000.m, R= 0. m, events/ton/3.8E20 POT

Solid, ν_μ events
Dashed, μ induced $\overline{\nu} bar_e$ events x100
Dotted, K induced $\overline{\nu} bar_e$ events x100

numuCC, Z= 1000.m, R= 0. m, events/ton/3.8E20 POT

Figure 3: Comparison of neutrino interaction rates for the 0.6° (11 mr) NUMI off-axis long-baseline detector (ME positive configuration, top plot), and the MINOS near detector for the LE (middle plot) and ME (bottom plot) positive NUMI beam configurations. ν_μ and electron neutrino [$(\nu_e + \overline{\nu}_e) \times$ 100] interaction rates are shown (the contribution from muon decays is is the dashed line and the contribution from kaon decays is the dotted line).

a short-baseline off-axis near detector can achieve a flux spectrum very similar to that in a low energy long-baseline off-axis beam, as illustrated in Figures 4 and 5.

In an off-axis near detector, the peak of the flux is wider because the neutrino source is not point-like at short baselines, but the peak energies and electron- neutrino backgrounds are very similar. Comparison between Figures 4 and 5 illustrates the fact that the desired energy in the off-axis detector can be tuned by a modest displacement in the direction perpendicular to the neutrino beam. Rates in off-axis near detectors remain high, with approximately 7×10^4 muon-neutrino interactions per ton-year between 1 and 3 GeV for the 2 GeV near off-axis beam shown in Figure 4.

Unfortunately, the significant difference in the flux spectra (between an on-axis and off-axis near detector) illustrated in Figure 3 compromises the usefulness of the currently planned NUMI [10] near detector for a future off-axis neutrino oscillation experiment. The primary purposes of a near detector in an oscillation experiment are the measurement of fluxes and cross-sections and studies of far detector perfor-
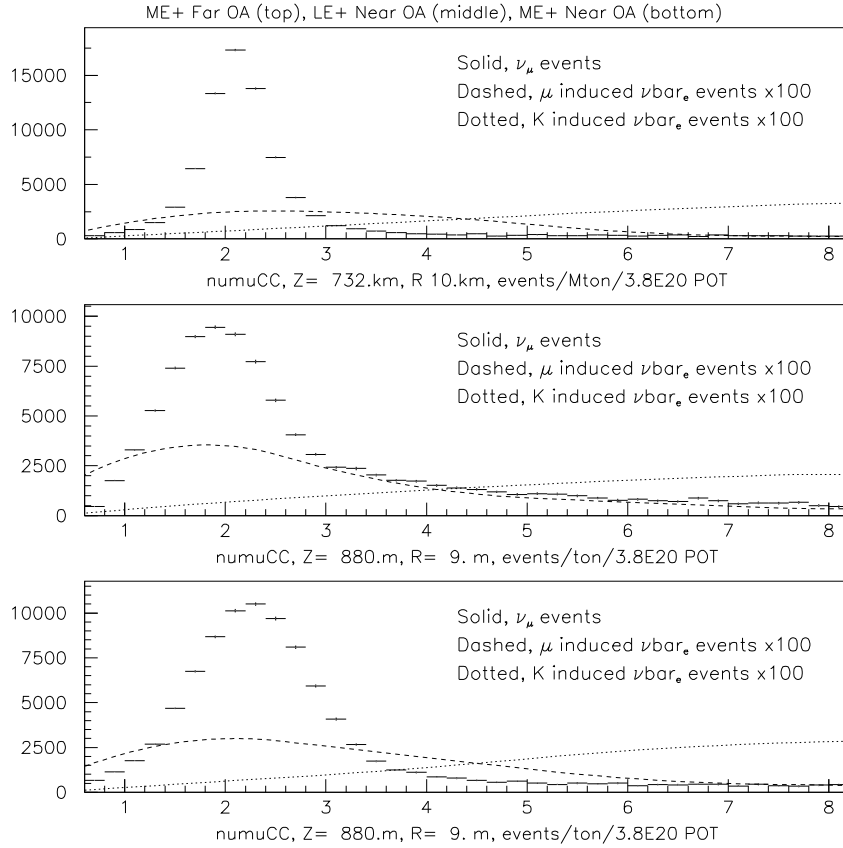
Figure 4: Comparison of neutrino interaction rates for a 0.6° (11 mr) NUMI off-axis long-baseline detector (ME positive configuration, top plot) and an off-axis near detector for the LE (middle plot) and ME (bottom plot) positive NUMI beam configurations. ν_μ and electron-neutrino [$(\nu_e + \overline{\nu}_e) \times 100$] interaction rates are shown. It is clear from the energy spectra that an off-axis near detector at 11 mr is very well suited for measuring neutrino cross sections in the 2 GeV region with either the LE or ME configurations (which have similar spectra).

mance. The fact that the planned on-axis near detector flux in the 1–2 GeV region is a tiny fraction of the total flux and that the detector is built to mimic the MINOS far detector, optimized for high energy neutrino reconstruction instead of measurement of exclusive final states, will make the currently planned on-axis near detector not suitable as a near detector for an off-axis experiment.

Upgrades or additions to the existing detector could address the issue of detector suitability, but the inherent difficulty of significant flux differences on and off axis remains. Of particular concern is the large on-axis rate of high energy neutral-current (NC) interactions, which have the potential to fake lower energy ν_μ and ν_e charged-current (CC) interactions. These high energy interactions, from the deep-inelastic regime, are qualitatively different than interactions near 1 GeV (the quasi-elastic region) or in the 2–3 GeV region (resonance inelastic region), as discussed in Section 3
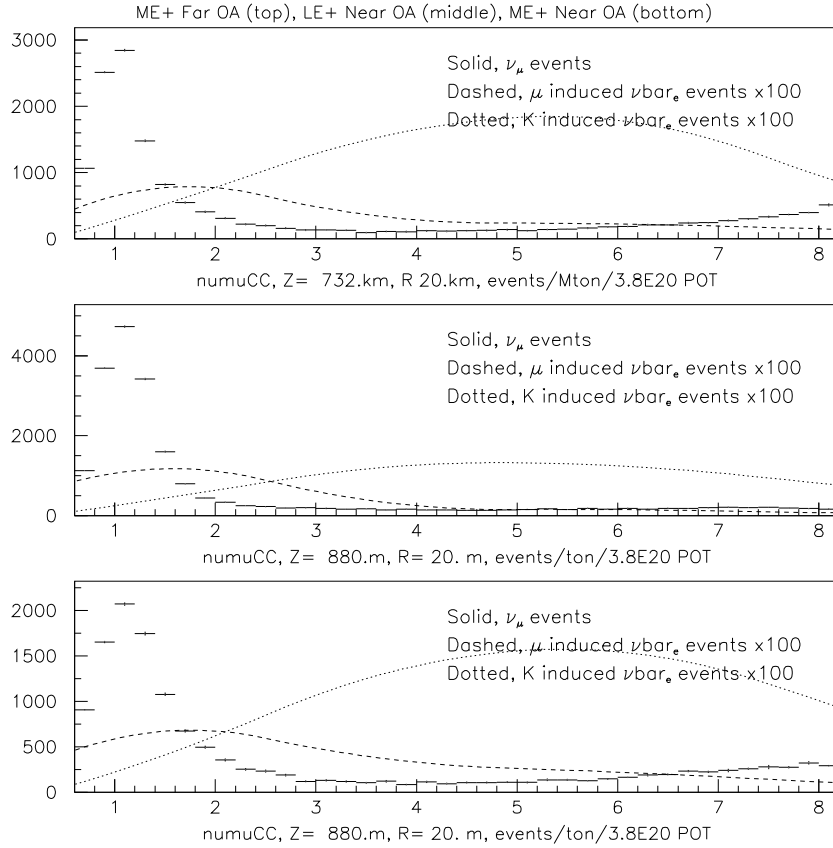
9

Figure 5: Comparison of neutrino interaction rates for a $1.5°$ (26 mr) NUMI off-axis long-baseline detector (ME positive configuration, top plot), and an off-axis near detector for the LE (middle plot) and ME (bottom plot) positive NUMI beam configurations. ν_μ and electron-neutrino [$(\nu_e+\overline{\nu}_e)\times 100$] interaction rates are shown.

2.1 Studies of Far Detector Backgrounds in a Near Detector

There are two backgrounds of primary concern in a long-baseline $\nu_\mu \to \nu_e$ experiment at low energy: NC interactions of high energy neutrinos and ν_e or $\overline{\nu}_e$ in the beam at the source. Figure 6 shows the rates of each background source (where no attempt has been made to reject the NC background). The background spectra of the off-axis near and far detectors are very similar, in marked contrast to the on-axis spectrum. As illustrated in Table 1, in the 1–3 GeV region of interest, the ν_μ charged-current rates in the on-axis detector are half that of the off-axis detector, while the absolute electron neutrino and neutral current backgrounds are a factor of 1.6 and 10 worse, respectively.

In addition, detailed investigation of the final states in neutral-current interactions, which is needed in order to understand the background in the far off-axis detector [1], is most simply done in a beam with the same energy spectrum as the far detector. For example, 2 GeV hadron showers that originate from the neutral current interactions of 3 GeV neutrinos have a different rate and composition than that of
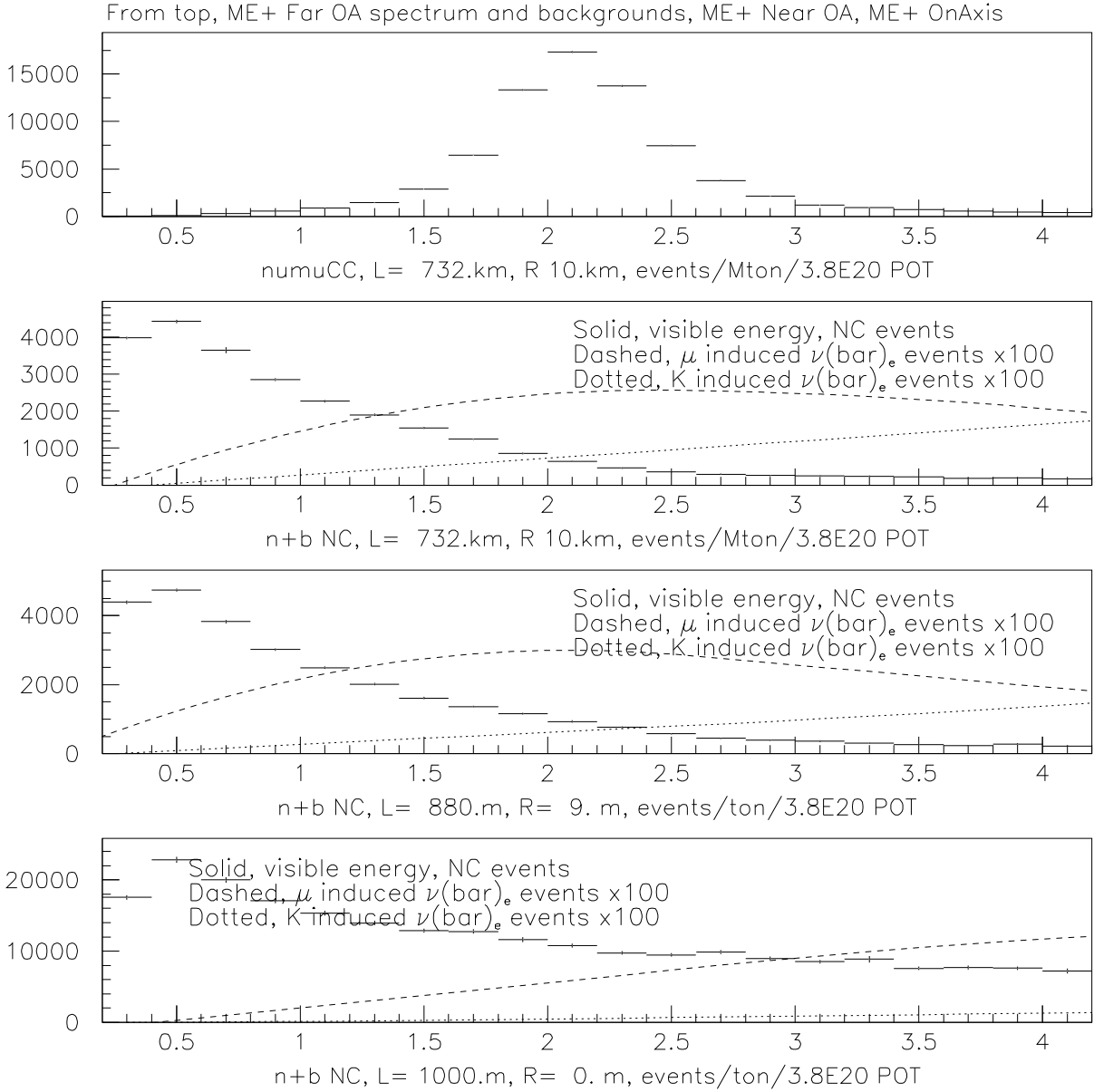
10

From top, ME+ Far OA spectrum and backgrounds, ME+ Near OA, ME+ OnAxis

numuCC, L= 732.km, R 10.km, events/Mton/3.8E20 POT

Solid, visible energy, NC events
Dashed, μ induced $\nu(bar)_e$ events ×100
Dotted, K induced $\nu(bar)_e$ events ×100

n+b NC, L= 732.km, R 10.km, events/Mton/3.8E20 POT

Solid, visible energy, NC events
Dashed, μ induced $\nu(bar)_e$ events ×100
Dotted, K induced $\nu(bar)_e$ events ×100

n+b NC, L= 880.m, R= 9. m, events/ton/3.8E20 POT

Solid, visible energy, NC events
Dashed, μ induced $\nu(bar)_e$ events ×100
Dotted, K induced $\nu(bar)_e$ events ×100

n+b NC, L= 1000.m, R= 0. m, events/ton/3.8E20 POT

Figure 6: Visible energy distributions of neutrino interactions at far and near detectors in a 0.6° (11 mr) NUMI off-axis beam (ME positive configuration). The top plot shows the neutrino energy for ν_μ interactions (no oscillation) in the long-baseline detector; the second shows visible energy for possible background sources, NC and electron neutrino interactions (the latter shown ×100). The third plot is the same background energy distributions for the off-axis near detector, and the last shows these distributions for an on-axis near detector.
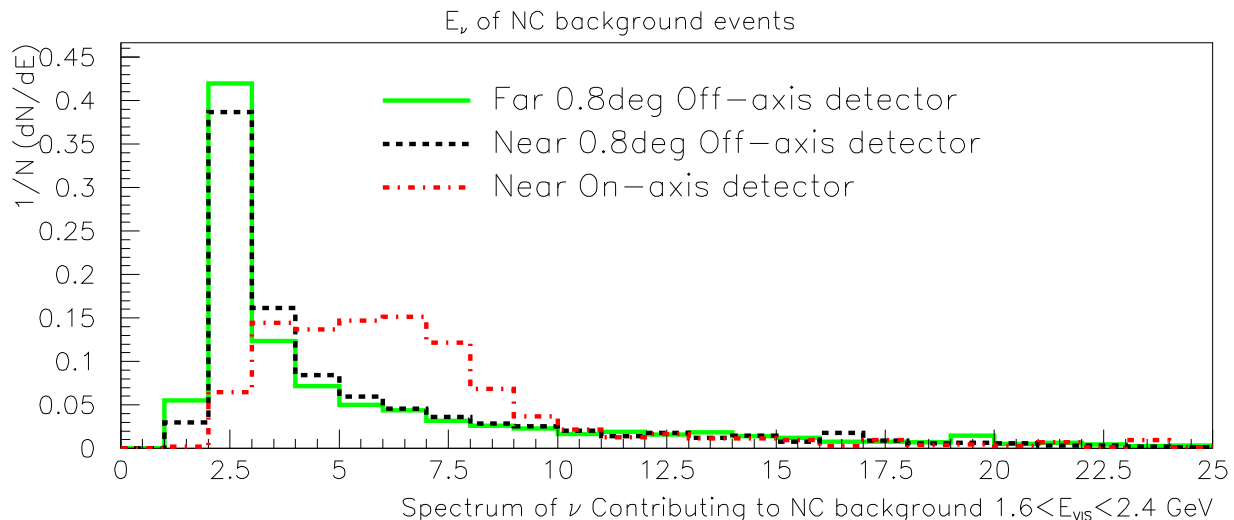
Figure 7: E_ν of NC events in a visible energy regime that contributes to long-baseline detector background in an 0.6° off-axis experiment (1.6–2.4 GeV)

2 GeV hadrons showers that originate from the neutral current interactions of 10 GeV neutrinos. The rate is a function of flux, energy, x, Q^2 and y, and the hadronic final state (e.g. fraction of neutral pions) is a function of the W and Q^2 of the interaction.

Figure 7 shows the neutrino energies contributing to NC background in the far detector peak for the far detector, off-axis near detector and on-axis near detector. The significant difference in neutrino spectrum responsible for NC background in the near detector indicates that the on-axis location will be difficult for investigating the misidentification rate of NC events as electron-neutrino events.

2.2   Anti-Neutrinos in Neutrino Beam

For the NUMI beam of positively focused mesons, the ν rate overwhelms the $\overline{\nu}$ rate, and makes it practically only a very small signal, as illustrated in Figure 8. Practically, as discussed in Section 4.2, there is little need for a magnet to measure the sign

Beam	Rate unit	$1 < E_{\text{vis}} < 3$ GeV		
		ν_μ (no osc.)	ν_e and $\overline{\nu}_e$	Neutral Currents
Far Off-Axis	events/kton-yr	69.5	0.34	9.9
Near Off-Axis	events/kg-yr	68.9	0.37	11.7
Near On-Axis	events/kg-yr	34.6	0.57	115.5

Table 1: Rates for signal and background processes with visible energy between 1 and 3 GeV in long baseline and near detectors in the 0.6° off-axis NUMI beam (ME positive configuration), compared with on-axis near detector rates.
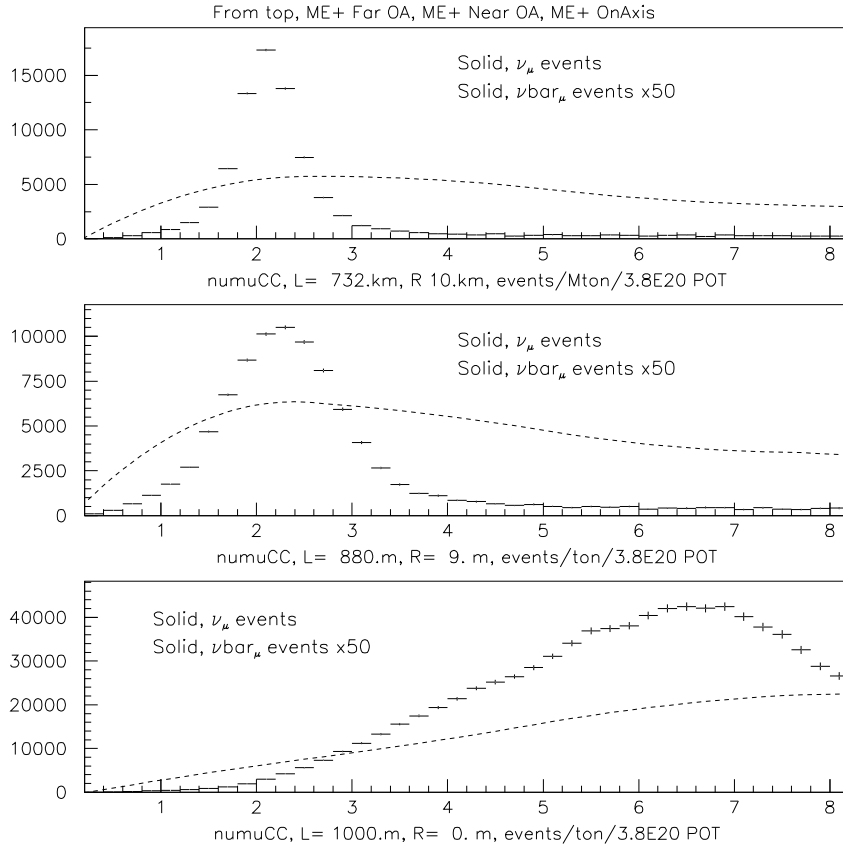
Figure 8: The ν_μ and $\overline{\nu}_\mu$ ($\times 50$) spectra at long-baseline and near off-axis $0.6°$ detectors, and in an on-axis near detector (ME positive NUMI beam).

of the final state muon. However, in a negatively focused beam, as shown in Figure 9, the story is quite different, where the wrong neutrino makes up $\sim 10\%$ of the rate at the peak.

3   Physics of Low Energy ν Cross-sections

The analysis of neutrino experiments in the ≈ 1 GeV and 2–3 GeV regions is very different. Below 1 GeV, the quasi-elastic cross sections dominate. Most experiments in this region, e.g., water Cerenkov experiments, can only observe the final state muon and are not sensitive to recoil nucleons. The energy of the events is obtained under the assumption that the reaction was quasi-elastic. Therefore for experiments in the 1 GeV range, background predictions require knowledge of how often inelastic scattering events look like a quasi-elastic events. In the 2–3 GeV region, the inelastic cross section dominates with a significant contribution from quasi-elastic events. In this energy region, the unobserved hadrons are very important. Even detectors which are sensitive to hadronic final states, e.g., sampling calorimeters, have a different response to charged and neutral pions. The energy calibration and the misidentifica-
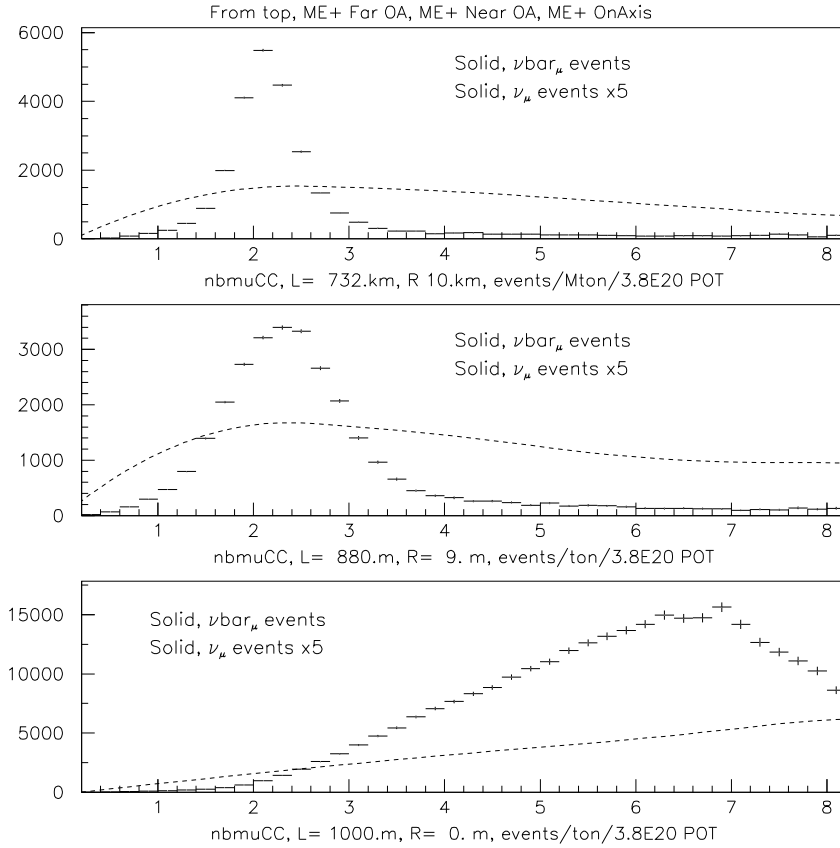
Figure 9: The $\overline{\nu}_\mu$ and ν_μ ($\times 5$) spectra at long-baseline and near off-axis $0.6°$ detectors, and in an on-axis near detector (ME negative NUMI beam).

tion of NC events as CC ν_e events is very dependent on the fraction and fragmentation function of neutral pions in the final state.

At present, the neutrino differential cross sections for CC and NC events, and the hadronic final states in the 2–3 GeV region are not well understood. The lack of good data in this region limits the physics capabilities of any future neutrino oscillations experiment. The measurements of interest are:

- Total and differential cross sections for charged current and neutral-current interactions with nucleons

- Hadronic final states in CC and NC interactions with nucleons

- Fermi motion and nuclear effects in the differential cross sections and hadronic final states

- Coherent nuclear processes

In each case, the current data in the 1–few GeV region has large uncertainties. As described below, theoretical models exist to characterize these reactions and relate νA scattering to well-measured eA processes. These models don't provide predictions for
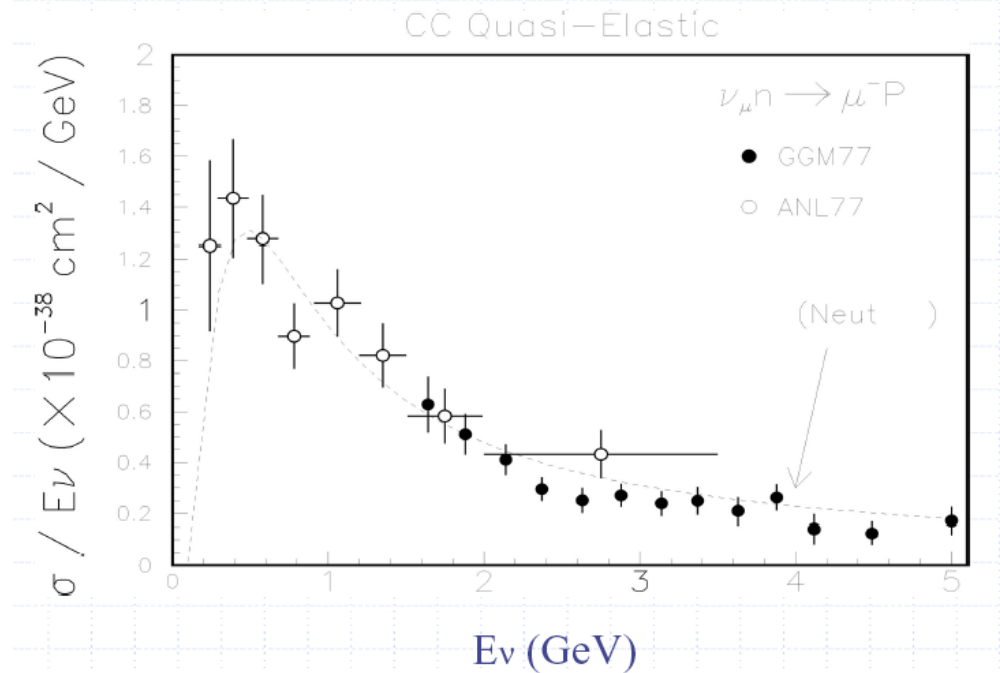
14

Figure 10: Neutrino quasi-elastic cross section data on neutrons.

neutrino scattering cross-sections and final states, but rather lend theoretical guidance to interpreting precise low energy data as it becomes available from measurements such as we describe.

3.1 Total and Differential Cross-sections

3.1.1 Quasi-elastic Scattering

The physics of quasi-elastic scattering [11] is described in terms of nucleon weak and electromagnetic form factors. Some information on form factors comes from electron-nucleon scattering and some from measurements with neutrinos. On nuclear targets, the effects of Fermi motion must be included. One commonly used calculation of the Fermi motion effects is that of Bodek and Ritchie [12], which includes the momentum distribution of nucleons within a Fermi gas model with the addition of nucleon-nucleon correlation and the effect of energy conservation of the remaining recoil nucleus. Although not sophisticated from a nuclear physics point of view, the approach taken is that the phenomenological parameters of the Fermi gas model are obtained from fits to electron scattering data on nuclei and applied to neutrino data within the framework of the same model. This is one example in which electron scattering data can be used directly in the modeling of neutrino scattering data.

Within the Bodek-Ritchie Fermi motion calculation, there are additional parameters that need to be tuned. The model is reasonable at low Fermi momenta, where a collection of spectator nucleons is recoiling against the interacting nucleon. Here however, one needs to model the excitation spectrum of the recoil spectator nucleus,

in order to properly account for energy conservation. At the other extreme, the high momentum components of the nucleon momentum distributions are not well known (they are usually modeled within a two-nucleon correlation model, and introduce an uncertainty into the calculation).

The best way to understand quasi-elastic processes on nuclear targets is to use the same model to do an analysis of data with both electrons and neutrinos on the same nuclear targets, within the framework of a nuclear model (e.g. Fermi motion, including a spectrum of spectator final states) and the best available nucleon vector and axial form factors.

The current data on quasi-elastic neutrino cross sections [13] are shown in Figure 10. As mentioned earlier, the largest errors come from trying to use these data for nuclear targets. Note that the modeling of quasi-elastic differential cross sections and final states requires knowledge of the total cross sections, the three weak form factors as a function of Q^2, Fermi motion and nuclear binding corrections, and final state interactions of the recoil nucleons.

3.1.2 Inelastic Scattering

In general, all inelastic scattering is described in terms of three structure functions $xF_1(W, Q^2)$, $F_2(W, Q^2)$ and $xF_3(W, Q^2)$. In the deep-inelastic region (high W) and at high Q^2, the relationship between the structure functions measured in electron and muon scattering and the structure functions in neutrino and antineutrino scattering are given in terms of Parton Distribution Functions (PDFs). In contrast, at low Q^2 and in the low W resonance region, a different language has been used including vector dominance models, resonance excitation form factors, production of exclusive channels etc. In addition, in the few GeV region, the relation between neutrino and electron scattering data has not been clear (because of the axial part in neutrino processes).

It has been well known that in the electron scattering case that there is a duality [14] between the cross section in the resonance region, and the in the deep inelastic region. The inelastic structure function $F_2(x', Q^2)$, if modified to use more sophisticated scaling variables, can describe the average cross section in the low W resonance region. In some analyses [15], instead of resonance excitation form factors [16], the resonances are treated as a final state interaction (as a function of W and Q^2) that modulates and introduces bumps and wiggles into the average cross predicted from the $F_2(x', Q^2)$ fits to deep inelastic data. Therefore, duality predicts that the formalism for deep-inelastic scattering should describe the average of the data in the resonance region, provided that more sophisticated scaling variables (e.g. x', x_w, ξ) are used and the low Q^2 higher twist effects could be taken into account. It was not clear if the higher twist effects in neutrino and in electron scattering were the same. However, recent work by Bodek and Yang [17] has shown that for Q^2 greater than 1 GeV^2, most of higher twist effects in electron scattering originate from final and initial state target-mass [18] effects and from the missing higher order QCD terms. Therefore, most of the higher twist effects in neutrino and electron scattering should be the same. Using this result Bodek and Yang [19] modified the leading order [20] GRV94 QCD PDFs (which already include QCD evolution down to $Q^2 = 0.25 \ GeV^2$
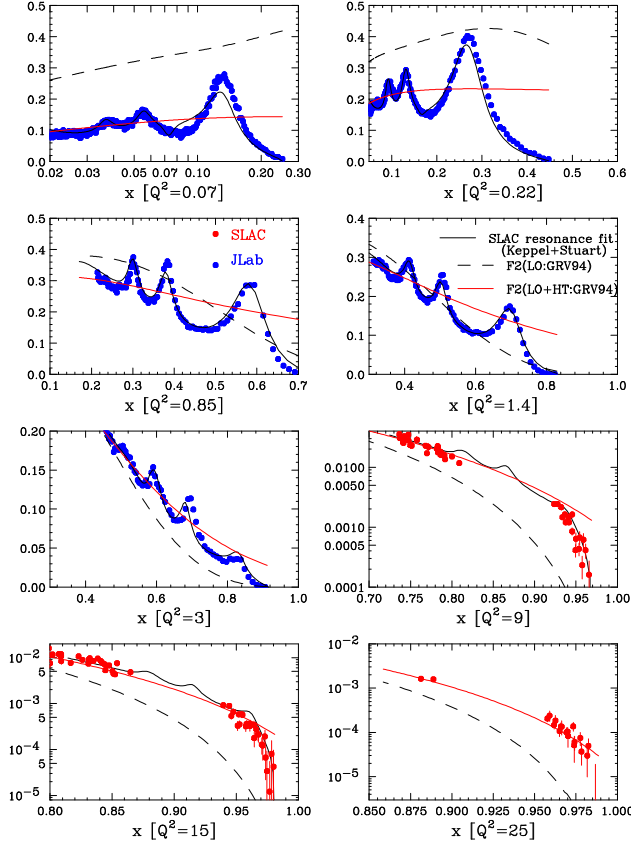
Figure 11: Comparison of a SLAC and JLab low energy electron scattering data in the resonance region (or fits to these data) and the predictions of the GRV94 PDFs with (LO+HT, solid) and without (LO, dashed) the Bodek-Yang modifications.

to include the higher twist effects (which originate from initial and final state mass effects and from the missing NLO and NNLO terms) in the form of another modified scaling variable [15] (x_w) such that the PDFs could be used all the way down to the photoproduction limit $Q^2=0$. The modified PDFs also describe the average of the low W cross section in the resonance region [21] for all available data at SLAC and Jefferson lab (down $Q^2=0.2$ GeV^2) as shown in Figure 11. Further refinements to the modified PDFs are needed, for example adding the resonance modulating function [15] $A(W, Q^2)$ and using different scaling variables for the u, d, and s quarks. These PDFs can then in principle also be used to predict neutrino and antineutrino differential cross sections for all energies.

The cross sections predicted by these modified PDFs can them be compared to measured low energy neutrino data to determine the deviations from this model. It is expected that there will be deviations from the model at very low Q^2 and low W because of the axial nature of the W boson, and because resonances of different isospin are produced at low W. In addition, at low Q^2 nuclear-effects in neutrino and electron scattering could be different.
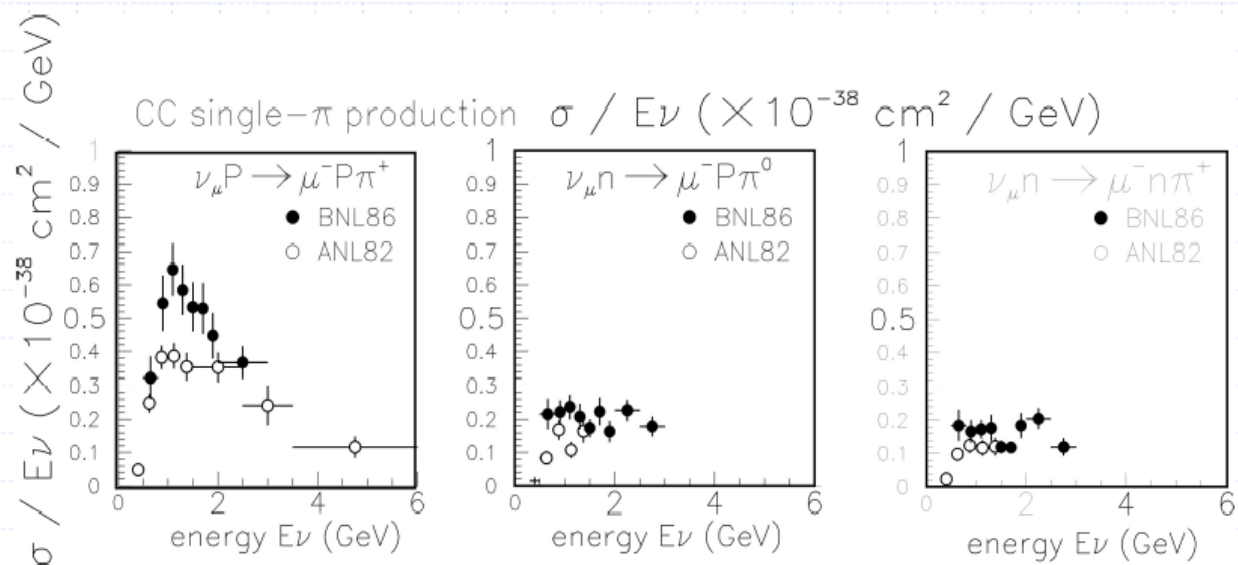
17

Figure 12: Neutrino charged current single pion production cross section data. Even in this simplest channel, the errors are large and the data are not consistent. Note that good measurements of both the total cross sections and kinematic distributions of all the final states are needed.

3.2 Hadronic Final States

Even if one has a complete description of electron scattering differential cross sections as well as neutrino charged-current and neutral-current differential cross sections at all W and Q^2, one needs to understand the hadronic final states. In a QCD language, the hadronic final states are described in terms of fragmentation functions of the final state quark (as a function of W and Q^2), which result from the color force between the final state struck-quark and the spectator quark (e.g. in the Lund string model). Or alternatively, the final states could be described in terms of the decay products of a final state mass W (e.g. a resonance), or as cross sections for production of exclusive final states (e.g. single pion production etc.). In either language, the fragmentation functions are functions of W and Q^2. Therefore, detailed measurement of final states in electron, muon, neutrino charged-current, and neutral-current scattering experiments on a variety of nuclear targets are needed in order to get a complete picture of the hadronic final states in all these reactions. As mentioned earlier, in the neutral-current case, an off-axis narrow band beam is needed since for such a beam, the initial energy spectrum of the neutrinos is relatively narrow.

The present available data on the neutrino cross sections for one exclusive final state (single pion production) and for the total cross section (sum of quasi-elastic and inelastic) are shown in Figures 12 and 13. As can be seen in the figures, data from different experiments are not in agreement and the errors are very large in this one channel. Note that in addition to the total cross section for such an exclusive process, the W and Q^2 distributions must also be know in order for these data to be useful. The fragmentation to one, two or more pions and nucleons needs to be known, as well
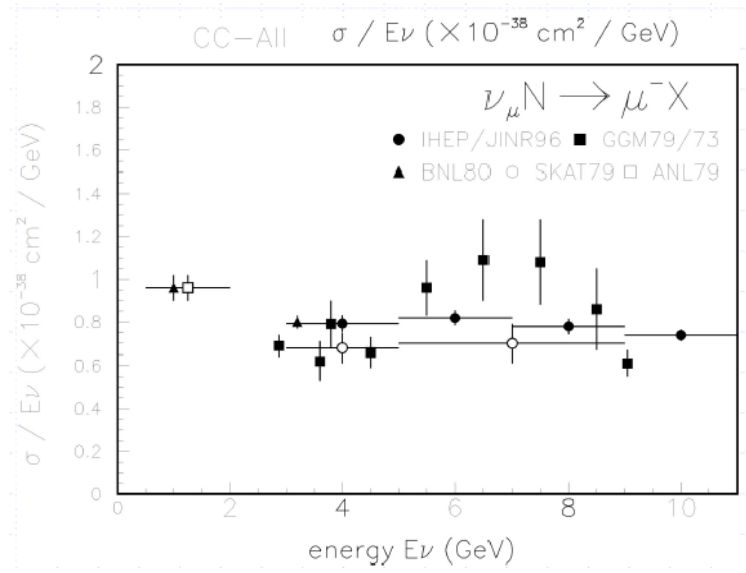
18

Figure 13: Neutrino total cross section charged-current data (quasi-elastic plus inelastic.

as the fraction of neutral and charged particles in the final state.

3.3 Fermi Motion and Nuclear Effects

The nuclear distortion of the inelastic structure functions (originating from Fermi motion, nuclear energy binding, and shadowing effects) have been measured in the deep inelastic region for the structure function $F_2(x, Q^2)$ in electron and muon scattering (Figure 14). Although not expected to be exactly true, most people have assumed that for the same value of x, these effects are independent of Q^2 or W and are the same for the three neutrino structure functions $2xF_1(x, Q^2)$, $F_2(x, Q^2)$, and $xF_3(x, Q^2)$. Therefore, measurements of nuclear effects with both electron and neutrino beams [22] at lower energies are needed.

There is not much data on nuclear effects on the fragmentation functions. These effects are expected to be significant and at low energies these may be different in neutrino, antineutrino, charged-current, neutral-current, and electron scattering. Neutral pions can be absorbed in the final state nucleus or converted to charged pions. Nucleons produced in quasi-elastic scattering can interact with final state nuclei and produce additional pions, etc. Therefore, both measurements with an off-axis near detector composed of a similar nuclear target material that is used in off-axis far long-baseline detectors, and an understanding of the nuclear effects are needed.

We have initiated discussions with scientists who do experiments in the Jefferson Laboratory about a collaborative effort in a combined analysis of neutrino and electron scattering data on hydrogen, deuterium and nuclear targets, as well as future participation in this off-axis low energy neutrino program at Fermilab. A coordinated program of measurements with neutrino and electron beams in the same energy range of all the above processes (with a variety of nuclear targets) is of interest. In principle, a measurement of nuclear effects in electron scattering experiments
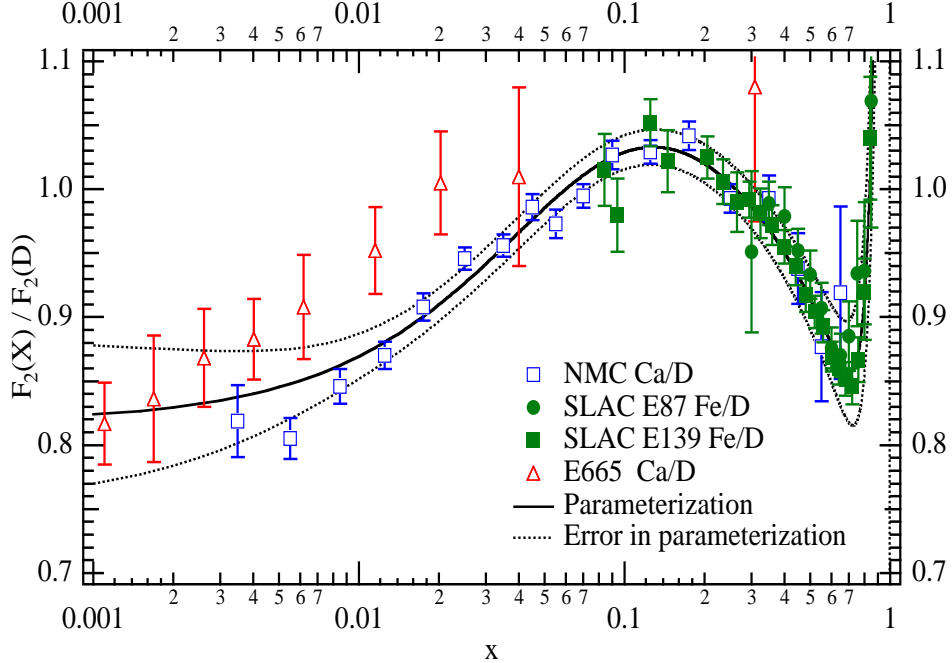
19

Figure 14: The ratio of $F_2(x, Q^2)$ data for heavy nuclear targets and deuterium as measured in charged lepton scattering experiments(SLAC,NMC, E665). The band show the uncertainty of the parametrized curve from the statistical and systematic errors in the experimental data [23]. At low Q^2 this ratio is expected be Q^2 dependent. In addition, in vector dominance models it is expected to be somewhat different in neutrino NC and CC and electron scattering reactions.

can be used as a first estimate in the "conversion" of neutrino data taken on carbon to predictions for data on a water target. As a check of this procedure, measurements of neutrino and antineutrino differential cross sections and hadronic final states with different nuclear targets are useful.

3.4 Coherent Nuclear Processes

Coherent particle production processes such as coherent neutral-current production of neutral pions ($\nu A \rightarrow \nu A \pi^0$) have to be modeled separately since these processes only occur on nuclei. The vector dominance models that are used to describe these processes need to be constrained by direct measurement with neutrino beams before they can be applied to predict enhancements to backgrounds to neutrino interactions on nuclear targets. Studying such processes on the relevant long-baseline target material would be possible in a near detector.

4 Detector Requirements

We discuss requirements of the detector as a whole and particular subsystems in order to provide the measurements of processes described in the previous section.

4.1 Energy Resolution and Calibration

Absolute neutrino cross sections are measured by dividing the observed number of events at a given visible energy by the predicted flux versus neutrino energy. Relative cross-sections in this type of experiment may be obtained by varying the detector position to vary the mean neutrino energy in a reliably predictable way. In either case, absolute calibrations to electromagnetic and hadronic final states will help to check the flux. In addition, the final state parameters (e.g. W and Q^2, y) need to be measured.

Relative calibrations of systems of the near detector can also be carried to the far detector to the extent that the two absorber and active detector are identical. Such a calibration is important in predicting backgrounds which are rejected by visible energy cuts, such as neutral currents.

4.2 Muon Charge Measurement

In neutrino running, the fraction of antineutrinos is $\mathcal{O}(1\%)$, but is approximately 10% in the antineutrino mode (see Sect 2.2). Therefore, one could conclude that sign determination could be delayed to a later stage, since most of the initial running will be done with a neutrino beam.

However, even in neutrino mode, the reaction

$$\nu p \to \nu \pi^+ n$$

may prose a significant background the quasi elastic $\nu n \to \mu^- p$ when the final state proton is nearly recoilless. The presence of a magnet in the initial running may therefore be helpful from the start, although this remains to be demonstrated by quantitative simulation.

4.3 Final State Identification

One of the goals is the determination of the cross sections for various final states for charged-current and neutral-current events. Muon and pion separation are required to distinguish, e.g., the reactions $\nu n \to \mu^- p$ and $\nu n \to \nu p \pi^-$. The reasonably active portion of the target will likely need to be long, several interaction lengths, to allow sufficient separation. For separation of electrons (from electron neutrino charged current interactions) from charged pions or neutral pions on an event-by-event basis, again an active target of many radiation lengths in order to convert photons and begin electron showers. Finally, observation of the direction and momentum of recoil protons in, e.g., the quasi elastic interaction $\nu n \to \mu^- p$ can be an additional important handle to reject backgrounds from processes like $\nu n \to \nu \pi^- p$.

4.4 Upstream Veto

An instrumented upstream veto is needed in order to define a clear longitudinal fiducial volume, shield the detector from incoming neutrons and photons and identify incoming muons. If this shielding is iron, the most downstream segments can provide a source of neutrino interactions on iron.

4.5   Target Material and Mass

Good energy resolution, tracking, and identification of very short range particles like recoil protons, requires a fully active target such as scintillator. The NUMI off-axis proposal suggests the far detector target material will be plastic or other similar hydrocarbons, or perhaps water[1]; the JHF neutrino project proposes to use a long-baseline water-Cerenkov detector[9]. This choice is made because of cost and because there is a natural preference for a low Z materials which give higher event rates for a given sampling in units of radiation lengths. There is interest as well in measuring low-energy cross-sections on iron because other long-baseline neutrino experiments, notably MINOS, use iron as their target material, but this target can be provided by the upstream veto as described below.

The mass of target material is driven by the needed statistical precision. A measurement likely limited by statistics is the comparison of the "fake" electron-neutrino rate in material of the far detector using only the sampling available in a far detector, to the rate of "real" electron neutrinos identified in the more active near detector. Electron neutrinos in the right energy range comprise about 0.4% of interactions, and the long-baseline experiments require predictions of backgrounds at a precision of approximately 5%[1, 9]. Approximately, then, we require > 400 true electron neutrino events, corresponding to a rate of 10^5 charged-current muon neutrino interactions. This can be accomplished for an 11 mrad off-axis detector (peak energy 2 GeV) with a 2 ton fiducial volume, or 2 m^3 of plastic scintillator.

As previously noted, the conversion of photons for π^0 identification in such a target requires at least a few radiation lengths of active material downstream of the fiducial volume. For a plastic scintillator target with a 40 cm radiation length, this implies 1 m of active target downstream of the fiducial volume.

4.6   Containment of Muons and Charged Pions

Measurement of the energy of final states containing muons and charged points requires a detector capable of containing these particles. In neutrino interactions on

θ (°)	E' (GeV)	Range (m)	Transverse Range (m)	Q^2 (GeV^2)
0	3.0	14.3	n/a	0.0
30	2.1	9.8	4.9	1.7
45	1.55	7.0	5.0	2.7
60	1.15	5.1	4.4	3.5
90	0.71	2.9	2.9	4.3
135	0.46	1.6	1.1	4.8
180	0.41	1.3	n/a	4.9

Table 2: Quasi-elastic final state muon energy from a 3 GeV incident neutrino for various laboratory angle θ in degrees. The total length of scintillator needed to range a muon and the transverse thickness required are also shown.

nucleons (neglecting Fermi motion and binding energy), at a given angle in the laboratory, the maximum energy of particles in the final state is that of the quasi-elastic final state muons with

$$E' = \frac{E_\nu}{1 + 2\frac{E_\nu}{M}\sin^2\frac{\theta}{2}}.$$

If energies of muons from quasi-elastic events at all angles are to be identified for, e.g., a 3 GeV incoming neutrino, the requirements for containment volume in plastic scintillator is shown in Table 2. As can be seen from the range numbers in the table, one meter of scintillator downstream is not sufficient, and a denser range detector or a combined magnetized range detector/iron spectrometer is needed, both downstream and at the sides of the detector.

5 Conceptual Design of Scintillator Target

The conceptual detector described below is designed to serve as an "existence" proof that a detector with the right properties can be built with existing technology. The parameters are based on scaling arguments from existing detectors, and the physics criteria described above. Optimization of size, segmentation versus costs etc will be done with a full simulation at the time of a proposal.

The requirements described in the previous section point toward a fully active scintillator target with fine segmentation. A fully active target yields good energy resolution and identification of all final state particles. Fine segmentation allows for the tracking of final state muons and pions, and the separation of the two photons from the decay of neutral pions. A similar detector is currently being built for near detector system of the K2K neutrino experiment [24] in Japan, which is running in a similar energy range (although with very low statistics and a wideband beam).

An schematic of the conceptual design is shown in Figure 15. It consists of an active target (Figure 16), followed by a sampling electromagnetic shower counter and a magnetized range detector. It is preceded by an upstream sampling iron scintillator target and an instrumented upstream active veto. A layout of individual components of one of the active-target detector planes are shown in Figure 17.

5.1 The Fully Active Target

The active scintillator target is $4 \times 4 \times 3$ m^3 with an inner fiducial volume is $1 \times 1 \times 1.9$ m^3 The basic design element is $75\,\hat{x}$ and $75\,\hat{y}$ planes of 2×2 cm^2 strips of plastic scintillator, 4 m long. The strips are read out on one side with wavelength shifter fibers which are placed in grooves along each strip. Each plane contains 200 strips.

5.2 Downstream Calorimeter and Muon Range Detector

Downstream of the target is a Fe-scintillator sampling electromagnetic calorimeter and a magnetized toroid iron scintillator range detector/muon spectrometer 4×4 m^2 in transverse dimension The total depth of the electromagnetic calorimeter and range
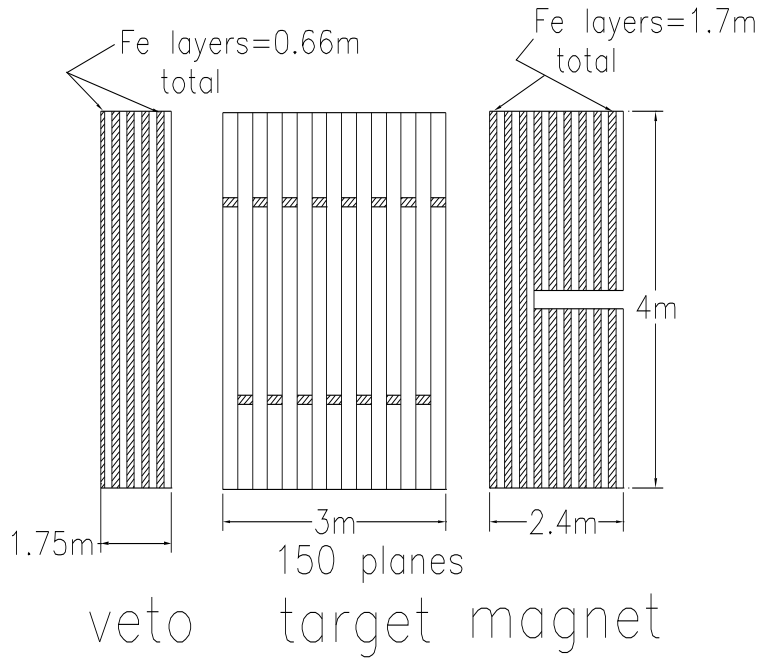
Figure 15: Conceptual layout of the components of the detector. A 4 m x 4 m active target, 3 m deep, is followed by a sampling calorimeter and magnetized range detector and preceded by an instrumented upstream veto.

detector is 1.7 meters of Fe. The first 20 Fe plates are 1 cm thick and serve as a 11.4 radiation length electromagnetic calorimeter. The remaining 1.5 m of Fe is magnetized and is sampled every 5 cm to contain and measure hadron energy and muon range. In this initial conceptual design the active material is the same planes as the active target, with alternating $\hat{x}$ and $\hat{y}$ samples.

As a solid iron magnetic spectrometer, the field would provide a P_t kick of 0.7 GeV/c, which is more than sufficient to determine charge. Since the dE/dx of a muon in iron is about 12 MeV/cm, a range measurement with a RMS of about 2 cm corresponds to an energy resolution (neglecting straggling) of about 25 MeV.

The entire electromagnetic calorimeter and magnetized range detector are shown in Figure 15 with a physical length of 2.4 m, including the sampling counters.

5.3   Upstream Veto and Iron Target

Upstream of the target is 65 cm thick iron 4×4 m^2 Fe-scintillator target/veto. It consists has an initial 20 cm passive iron shield, followed by 5 1 cm planes with active scintillator strip planes as in the active target. The fiducial volume of this target/veto in its use for studying neutrino cross-sections on iron would be $0.4 \times 2 \times 2$ m^3 or 12.8
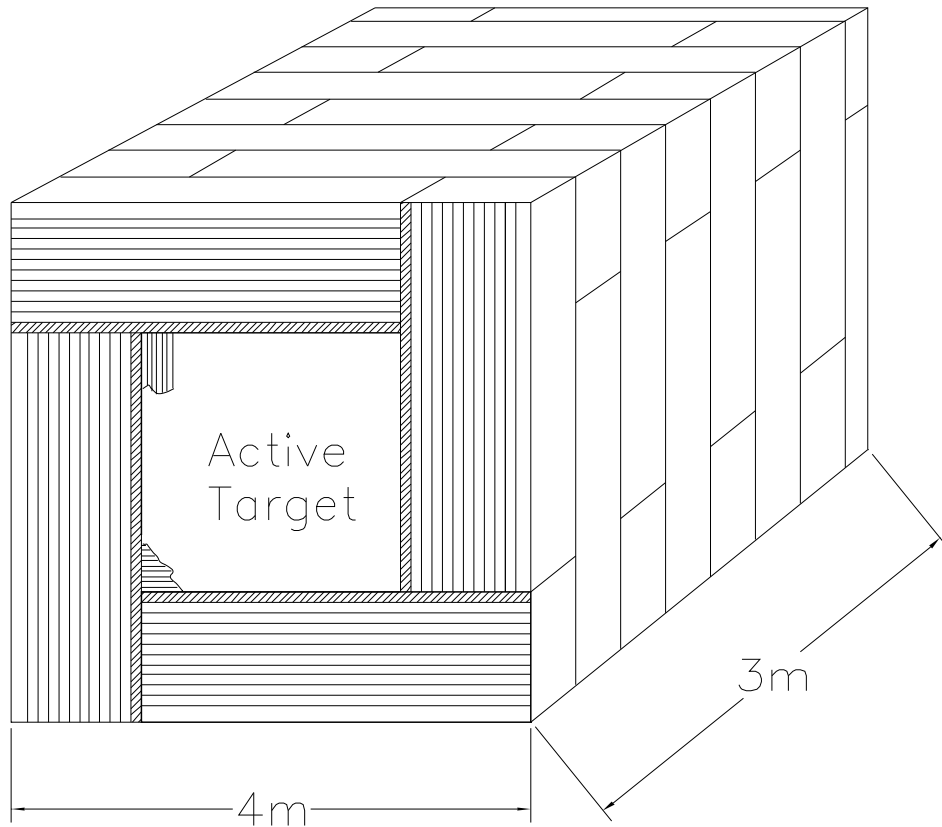
Figure 16: The beam's view of the active target. In each plane, the inner 2×2 m section is solid scintillator strips; the outer 1 m on each side consists of mixed scintillator and steel bars as described in the text.

tons. The total length is 1.75 m, including the active material.

Another option for the active portion of this veto would be to replace it with material from a long-baseline far detector if the absorber there is not carbon.

5.4   Mimicking a Long Baseline Detector

If the far off-axis detector design is chosen to be plastic with RPC chambers every 0.3 radiation lengths[1], then such chambers can be inserted into the active target every 16 cm for studies of far detector response in the more controlled environment of the near detector. (The total number of RPC chambers in this scenario is only 20). This example can be generalized to other long-baseline active detector choices.

5.5   Adding Absorber to the Active Target

Recall from the previous discussion of containing electromagnetic showers and muons that a solid scintillator detector would need to be too wide transversely to be practical.
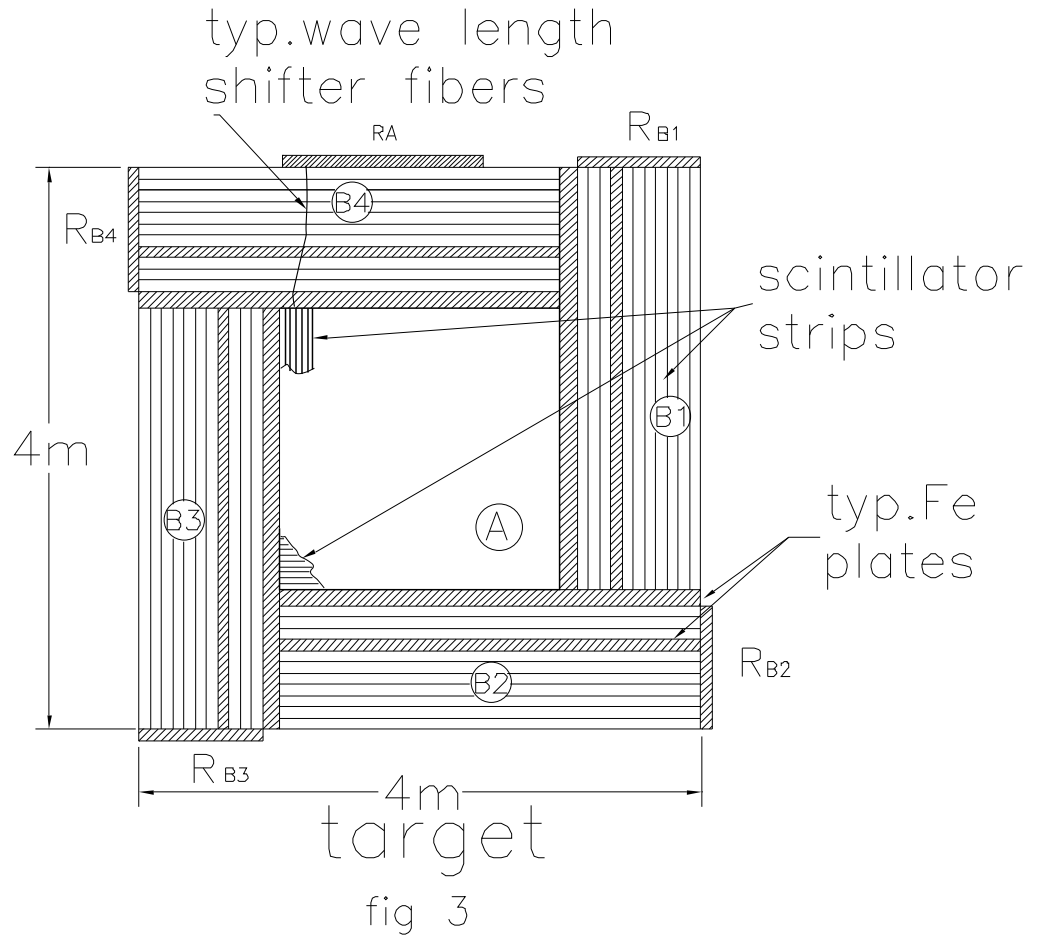
Figure 17: One plane of the active target. Locations of readout are shown marked with "R" in the diagram.

To reduce detector size, this conceptual design allows for the replacement of some of the active material in the outer portions of the detector with steel absorber strips of an identical cross-section, as illustrated in Figures 16 and 17. The inner 2×2 m^2 area in this concept is solid scintillator (region A in Figure 17). Four identical scintillator/steel absorber sections are shown as regions B1-B4, completing a 1 m thick "picture frame" around the fully active inner region. The inner 20 strips (40 cm total) of the 1 m thick "picture frame" are configured to make an electromagnetic calorimeter by alternating between 2 cm thick iron strips and 2 cm thick scintillator strips. The outer 30 strips (60 cm total) are configured as a muon range detector and would be constructed of 5 units, each with 5 iron strips followed by a single scintillator bar.

The counter planes are all read on one side from the regions marked with "R" in Figure 17. An advantage of the above design is that all the planes are constructed in the same way. When placed in the target, the planes are rotated by successive 90 degrees to form a pattern of x, y, x, y planes which are read out on alternate sides.

This design is flexible and allows the inner part of this active detector to be replaced with any type of target material (active or passive).

5.6 Total Materials and Components

The total active area in scintillator for this design of the target is accomplished with 15000 2 m long strips (2×2 cm^2, as always), and 9000 3 m strips. The iron absorber is provided by 21000 3 m long 2×2 cm^2 strips.

If the active scintillator detectors for the 100 sampling planes of the downstream calorimeter and range detector and the upstream veto consisted of 4 m long scintillator strips, 20000 would be required, dominating the scintillator volume. Almost certainly, more coarse segmentation, and perhaps alternate technologies, such as RPCs in the range stack can be used here to reduce costs in scintillator and readout.

5.7 Including Additional Active or Passive Materials

An optimized solid scintillator strip target-detector could certainly providing the detailed information needed about neutrino charged-current and neutral-current cross sections and final states in carbon in the few GeV region. This detector, with the addition of RPCs, is also excellent for mimicking the far detector with hydrocarbon absorber/RPC readout[1].

If a far detector technology that is chosen is water in plastic square tubes as the target material, and liquid scintillator in plastic tubes for the readout[1], the off-axis near detector design should also include measurements in water. Such a measurement also of interest for neutrino oscillation experiments planned or ongoing using large water Cerenkov long-baseline detectors [9, 24].

A measurement with water can be accomplished by replacing the iron with in the upstream veto/target with 2×2 cm^2 tubes filled with water, including a water based scintillator, and a wavelength shifting fiber. There are several commercially available [25] water soluble scintillators which either stay in liquid solution or convert the water into a gel[1]. Unfortunately, water based scintillators have significantly lower light output than solid plastic scintillator. Additional R&D on water based scintillators, or water based scintillating gels could be pursued. Alternatively, the high quantum efficiency [26] of VLPCs could be used to compensate for the reduced light yield of water based scintillators.

6 Conclusions

We have outlined the motivation for a near off-axis detector in the NUMI beam at Fermilab. A first attempt at a conceptual design indicates that such a detector can be built with existing technology. Data taken with such a detector in the 1–3 GeV region is essential for future neutrino experiments at Fermilab, Europe and Japan.

Since such an experiment is essential for the future of all neutrino oscillations experiments, it will be done either in the USA, Japan or Europe. Since Fermilab plans to have the first high intensity low energy neutrino beam, it is most expeditious

---

[1]At present, most of the usage of such scintillators has been for medical applications and for the measurements of radioactivity in water. However, choosing a scintillator suitable for applications in high energy physics requires further study.

and efficient for the international community to do this experiment at Fermilab. By initiating this program, Fermilab can begin to take a leading role in the future of neutrino physics in the next 20 years.

6.1   Next Steps

Following an encouraging response to this EOI, we would form a collaboration to write a more detailed LOI including the design and optimization of the detector, simulation and cost estimate.

References

[1] `http://www-numi.fnal.gov/fnal_minos/` `new_initiatives/new_initiatives.html`

[2] P. Fisher, B. Kayser, K. McFarland, Ann. Rev. Nucl. Part. Sci. **49** 481 (1999).

[3] Y. Fukada *et al.*, Phys.Rev.Lett. 81 (1998) 1562.

[4] SNO Collaboration, `nucl-ex/0204008`, `nucl-ex/0204009`.

[5] A. Aguilar *et al.* [LSND Collaboration], anti-nu/e appearance in a anti-nu/mu beam," Phys. Rev. D **64**, 112007 (2001).

[6] M. Apollonio *et al.*, Phys.Lett. **B466** (1999) 41.

[7] F. Boehm *et al.*, Nucl.Phys.Proc.Suppl. 91 (2001).

[8] V. Barger *et al.*, "Neutrino Oscillations at an Entry-Level Neutrino Factory and Beyond", `hep-ph/0003184`.

[9] Y. Itow *et al.*, "The JHF-Kamioka Neutrino Project", `hep-ex/0106019`.

[10] http://www-numi.fnal.gov/

[11] T. Kitigaki *et al.*, Phys. Rev. D**28**, 436 (1983).

[12] A. Bodek and J. L. Ritchie, Phys. Rev. **D23** 1070 (1981).
A. Bodek and J. L. Ritchie, Phys. Rev. **D24** 1400 (1981).

[13] see talk by M. Sakuda at NuInt01, the First International Workshop on Neutrino-Nucleus Interactions in the Few GeV Region, Dec. 2001, KEK, Tsukuba, Japan. To be published in Nucl. Physics B. Proceedings Supplement, Fall 2002. http://neutrino.kek.jp/nuint01/

[14] E. D. Bloom and F. J. Gilman, Phys. Rev. Lett. **25**, 1140 (1970).

[15] A. Bodek *et al.*, Phys. Rev. D**20**, 1471 (1979).

[16] D. Rein and L. M. Sehgal, Annals of Physics **133** 79 (1981); R. Belusevic and D. Rein, Phys. Rev. D **46**, 3747 (1992).

[17] U. K. Yang and A. Bodek, Phys. Rev. Lett. **82**, 2467 (1999).
U. K. Yang and A. Bodek, Phys. Rev. Lett. **84**, 5456 (2000); U. K. Yang and A. Bodek, Eur. Phys. J. **C13** 245 (2000).

[18] H. Georgi and H. D. Politzer, Phys. Rev. D**14**, 1829 (1976).

[19] A. Bodek and U. K. Yang, "Modeling deep inelastic cross sections in the few GeV region," hep-ex/0203009. Presented by Arie Bodek at NuInt01, the First International Workshop on Neutrino-Nucleus Interactions in the Few GeV Region, Dec. 2001, KEK, Tsukuba, Japan. To be published in Nucl. Physics B. Proceedings Supplement, Fall 2002

[20] (GRV94) M. Gluck *et al.*, Z. Phys. C**67**,433 (1995).

[21] C. S. Armstrong *et al.* (JLAB), Phys. Rev. D**63**, 094008 (2001).

[22] J. Marteau, "Effects of the nuclear correlations on the neutrino-nucleus interactions", submitted to the proceedings of NuInt01. http://neutrino.kek.jp/nuint01/

[23] W. G. Seligman, Ph.D. thesis, Columbia Univ., Nevis reports 292 (1997).

[24] Near Muon Range Detector for the K2K Experiment -Construction and Performance Nucl.Instrum.Meth. A482 (2002) 244-253 (hep-ex/0107041)

[25] Water soluble scintillators (e.g. LS8-NE220; LS-11- NE 221 gel; LS-84- Unisolve) are available from www.amcrys-h.com, 60, Lenin Ave, Kharkov 310001, Ukraine Tel. 380(572)307906 Fax 380(572)321082. E-mail:amcrys-h@amcrys-h.com. Liquid water soluble scintillators for biological applications (e.g. unisolve and others) are available from several vendors, including NBS Biological www.nbsbio.co.uk/chem6.htm. For scintillators for radiological tests of radioactivity in water see: http://www.npl.co.uk/npl/clubs/nlsuf/nlsuf1.pdf).

[26] P. Baringer *et al.* [D0 Collaboration], "Cosmic ray tests of the D0 preshower detector," Nucl. Instrum. Meth. A **469**, 295 (2001).